X-612-64-389

NASA TMX-55183

MAGNETIC FIELDS: REASONS FOR SIMULATION METHODS AVAILABLE

BY
NORMAN F. NESS

DECEMBER 1964

NASA
GODDARD SPACE FLIGHT CENTER
GREENBELT, MARYLAND

MAGNETIC FIELDS:

REASONS FOR SIMULATION AND METHODS AVAILABLE

by

Norman F. Ness

NASA-Goddard Space Flight Center

Greenbelt, Maryland

December 1964

Presented at Virginia Polytechnic Institute, Conference on the Roll of Simulation in Space Technology, August, 1964

Magnetic Fields: Reasons for Simulation and Methods Available

Norman F. Ness
NASA-Goddard Space Flight Center

Introduction

Magnetic fields are among the most ubiquitous of physical phenomenon studied by man. They are important on an atomic level in which magnetic field strengths of thousands of gauss are employed in the study of atomic structure. In cosmic physics stellar magnetic fields of tens and hundreds of gauss are important factors controlling the physical phenomenon observed. In interstellar and in interplanetary space magnetic fields of less than 10^{-4} gauss are important in determining the motion of charged particles and in the dynamics of the interstellar and interplanetary medium. The major portion of this talk is to be directed towards a description of the present spatial environment of the Earth with respect to magnetic fields. Following the descriptive aspects of the magnetic field as observed by satellite and space probes, the quantitative representation of these fields will be given. Finally a description of the presently available systems to simulate the magnetic fields in space will be reviewed and the most recent large scale facility for such work discussed.

The last section of the paper deals with engineering applications of our knowledge of the earth's magnetic field in various satellite programs. Certain of these applications are quite unique and represent some of the reasons for necessitating simulation of magnetic fields as observed in space. The unit of magnetic field force as commonly used in geomagnetism is the gamma (equal to 10^{-5} Gauss). On this scale a current of one

milliampere flowing in an infinitely long wire creates a magnetic field whose strength is 20 gammas at a distance of one centimeter.

There are a number of scientific reasons for mapping the magnetic field environment of the earth. These include:

1. Investigation of secular changes and the present state so as to determine the sources of the geomagnetic field and the interplanetary magnetic field structure;
2. To study and analyse charged particle motion which requires a knowledge of the geomagnetic and interplanetary magnetic fields, and
3. To determine the time variations of these fields and their correlation with auroral phenomenon, and solar activity.

In order to successfully map the magnetic fields in space it is necessary to perform direct measurements of the magnetic field from satellites and space probes. Thus they represent portable laboratory platforms upon which instruments sensitive to magnetic fields are placed. One of the primary engineering reasons for simulating magnetic fields in space is to test and calibrate the magnetometer sensors which will be used to directly measure magnetic fields in space. A second objective is to allow a measurement of the magnetic properties of satellite and space probes to determine:

1. Their contaminating or noise effects on magnetic field measurements made by magnetometers on board the same spacecraft,
2. To determine the dynamic interaction of the moving and possibly spinning spacecraft with magnetic fields, principally the earth's field and
3. To allow the testing of specific orientation and attitude control and spin producing subsystems which employ the geomagnetic field for magnetic torque interactions and/or directional information.

As more is learned about the magnetic fields in space more sophisticated use in an engineering sense can be made of this valuable information. The principal techniques of simulating terrestrially the weak magnetic fields which exist in space employ large current carrying coil systems which generate steady magnetic fields canceling the earth's field over a small volume.

Results of Magnetic Field Measurements in Space

A number of satellites carrying magnetometers have been launched by both this country and the USSR. A summary of those satellites measuring principally the earth's magnetic field is shown in Figure 1. In general the life time of these satellites has been individually limited as shown in Figure 2, summarizing trajectory characteristics pertinent to mapping of the earth's magnetic field. A very limited number of space probes have investigated the interplanetary magnetic field. In order to measure the properties of the interplanetary medium, undisturbed

by the presence of the Earth, it is necessary to perform measurements at a considerable distance from the surface of the earth. The interaction of the solar plasma resulting from the expanding solar corona[1] requires that these measurements be performed at least 80,000 Km from the earth near the subsolar point and at a considerably larger distance away from this region. As shown in Figure 3 those satellites which have performed measurements of the interplanetary field were quite limited either in accuracy or in measuring only a limited characteristic of the field and not the complete vector magnetic field.

A representative sample of the results of measurements in space confirming the general characteristics of the dipolar geomagnetic field is shown in Figure 4. The Explorer X satellite[2] carried a rubidium vapor magnetometer and performed successful measurements of the earth's magnetic field from 2 to 7 R_e (Earth radii) in March 1961. In Figure 4 are summarized both the direct measurements and the differences between the observations and the theoretical field values predicted by extrapolation using spherical harmonic analyses of the surface terrestrial field. It is seen that the deviations are quite small and represent less than 5 percent of the ambient field. However, these small deviations of the earth's magnetic field are extremely important in this region of space. It is precisely within this radial distance range that the trapped charged particle fluxes are

observed to reach their peak intensities.[3] The deviations observed, as illustrated in Figure 4, are consistant with the magnetic effects of charged particle spiral and drift motion in the earth's magnetic field. At the present time detailed models of the particle belts are being developed as more refined instrumentation permits investigation of the spectral and pitch angle distributions of energetic particles within the belts.[4]

A substantially different result in measuring the earth's magnetic field results when one considers Figure 5. The magnetic field results as obtained on the IMP-1 satellite[5] are shown near the subsolar point. It is seen that the earth's magnetic field agrees reasonably well with that predicted by spherical harmonic analysis until a distance of 7 or 8 R_e is reached. Beyond this point the observed field becomes increasingly stronger until a distance of 10.7 R_e is reached. At this point the measured magnitude of the field is approximately twice that predicted by theoretical analysis. Subsequent to this point on the trajectory the field abruptly drops to low and fluctuating values. This characteristic abrupt decrease of the earth's magnetic field following a gradual but significant increase in magnetic is identified as a boundary of the earth's magnetic field. It is due to the flow of solar plasma much in the fashion suggested by Chapman-Ferraro[6] more than 30 years to explain transient variations of terrestrial fields following solar activity.

A naive and simplified approximation to the very complex interaction of the solar plasma impacting the earth's magnetic field is shown in Figure 6. Here specular reflection from the boundary of the earth's magnetic field is assumed for the individual particle trajectories. Within this bounding region the dominant magnetic field is that of the earth's and the distortion of the geomagnetic field by currents on the containing boundary. This region of space has been referred to as the magnetosphere by Gold[7] since the motion of charged particles is completely dominanted by the earth's magnetic field. On the assumption of direct impact of the solar plasma on the earth's magnetic field, the stand off distance of the boundary, depending upon the solar plasma momentum flux and geomagnetic field strength, can be predicted. Figure 7 summarizes a parameter distribution of stand-off distances as a function of particle densities and energies. In order to convert from these values to fluxes one multiplies particle density by the equivalent proton velocity. The fluxes being discussed have been measured by space probes and satellites, but this paper does not intend to review this material. Interested readers are referenced to the papers by Snyder and Neugebauer, 1963[8]: Bonetti et al. 1963[9]; and Bridge et al. 1964.[10] The observed distance of 10.7 R_e and estimated plasma velocities of 300 to 700 Km/sec leads to plasma densities of 1 to 10 protons per cubic centimeter. A general summary of the present field

environment illustrating the relative position of the radiation belts in the magnetosphere is shown in figure 8. This illustration also shows the position in which the Explorer X satellite probe mapped the magnetic field of the earth and detected only small differences between theoretical and observed magnetic fields.

The results of the IMP-1 magnetic field experiment for out bound orbit number 15 is shown in Figure 9. The similar characteristic of a gradual increase in the strength of the observed field , over and above that predicted, is clearly seen. Beyond this, a region of rapidly fluctuating and low magnetic field strength is observed to extend to a distance of 23.1 R_e. Beyond this distance the magnetic field is reasonably steady and stable in orientation. We identify this abrupt temination of the fluctuating or tubulent region as a collisionless magnetohydrodynamic shock wave[11] associated with the interaction of the solar plasma with the earth's magnetic field. Our present understanding of this phenomenon is principally based upon an analogy with high speed gas dynamics.[12] In a fluid, disturbances can be propagated at a sensible velocity characteristic of the medium. In gas dynamics it is the acoustic velocity while in magnetohydrodynamics in which ionized gases are in motion the appropriate velocity is the Alfvén speed. This is shown in figure 10 as a function of particle density and magnetic field strength.

The average magnetic field strength in interplanetary space has been measured to be approximately 5 gammas[13] with extreme values between 1γ and 10γ . Particle densities between 1 and 10 protons per cm^3 lead to an Alfvén velocity in general less than 100 Km/sec. Direct measurements of the plasma velocities in interplanetary space indicate velocities on the order of 400 Km/sec. or more, and thus the flow of solar plasma is super Alfvénic with respect to the propagation of characteristic disturbances in the medium. On this basis the interaction of the earth's magnetic field with the solar plasma becomes much like that of a blunt object in supersonic gas flow in which a detached shock wave preceeds the body. It is separated from the obstructing article, which in this case is the magnetosphere boundary and not the earth's surface. A summary of the magnetic field environment of the earth in cis-lunar space is shown in figure 11. This is based upon the first 19 orbits of the IMP-1 satellite, which is the first satellite to have performed detailed and accurate measurements of both the magnetosphere boundary and the collionless shock boundray.

Three regions of space,

1. Magnetosphere
2. Turbulent Boundary layer and
3. Interplanetary medium

are representative of the characteristic aspects of magnetic fields which must be simulated on the surface of the earth. The important conclusion deduced from these data is that very weak

magnetic fields are observed in space and must be simulated on the surface of the earth. In addition it also implies that the "portable laboratory bench" upon which magnetometer sensors are placed must be very clean in the magnetic sense so that accurate measurements will be performed.

Geomagnetic Field Representation

In a region of space containing no sources of magnetic flux the magnetic vector F is derivable from a potential V which is a solution of Laplace's equation. In a spherical coordinate system (R, θ, ϕ) represent geocentric distance, colatitude and longitude east of Greenwich. The potential V can be represented in terms of a series of spherical harmonic function as

$$V = R_e \sum_{n=1}^{\infty} \sum_{m=0}^{n} P_n^m(\cos\theta) \left\{ \left[G_n^m \cos m\phi + H_n^m \sin m\phi \right] \left(\frac{R_e}{R} \right)^{n+1} + \left[\bar{G}_n^m \cos m\phi + \bar{H}_n^m \sin m\phi \right] \left(\frac{R}{R_e} \right)^{n} \right\} \quad (1)$$

in which

R_e = 6371.2 kilometers, equivalent radius of a spherical Earth

P_n^m = the partially normalized associated Legendre polynomials introduced by Schmidt and utilized in classical geomagnetism.[14]

G_n^m, H_n^m = harmonic coefficients for sources internal to spherical surface ($R = R_e$) with the dimensions of magnetic force

$\bar{G}_n^m$, $\bar{H}_n^m$ = the harmonic coefficients for sources external to the spherical surface ($R = R_e$) with the dimensions of magnetic force.

From the potential representation the magnetic field $\vec{F}$ is derivable as the negative gradient, $\vec{F}$ = -grad V, which yields straight forwardly the X, Y and Z or southward, eastward and radially outward components of the earth's magnetic field. Other elements common in geomagnetic field analyses are the horizonal and vertical components and declination of the magnetic field. There exist at present 10 sets of spherical harmonic coefficients for this analytic representation, all differing slightly.[15] In general $\bar{G}$ and $\bar{H}$ are small (of the order less than 3% of G and H) but become very important at satellite altitudes greater than 5 R_e.

The familiar approximation to the earth's magnetic field utilizing a centered dipole is based on the following values of harmonic coefficients:

G_1^0 = 30470 gammas

G_1^1 = 3030 gammas and H_1^1 = 45770

Using only these terms the observed magnetic field can be predicted within an accuracy of 87 to 91 per cent at geocentric distances of up to several earth radii. These values of coefficients correspond to a centered dipole titled 12^0 with respect to the earth's rotational axes and at a longitude 297.7^o east of Greenwich with an equivalent surface magnetic field

at the equator of 31,159 gammas. This is obtained from Vestine's model A for 1955 which is the best of all simple dipole coefficients. It is possible to represent the earth's magnetic field by an eccentric dipole which improves upon the accuracy and utilizes the first eight coefficients in a spherical harmonic expansion. In this representation the centered dipole is replaced by a dipole displaced from the center of the earth by 436 kilometers and intersecting the surface of the earth at

$\theta_n = 8.1^o$ $\qquad$ $\theta_s = 165.6^o$

$\Phi_n = 275.4^o$ E $\qquad$ $\Phi_s = 120.4^o$E

Use of this representation yields accuracies of the order of 90-96% for altitudes less than several R_e. At present most current students of the geomagnetic field have used coefficient sets with less than or equal to 63 elements corresponding to n and m being less than 6 (one exception utilized 512 coefficients). However, the impact of the solar wind leads to a distortion of the earth's field which at geocentric distances greater than 5 R_e contributes a significant portion of the observed magnetic field. This has been studied by Beard and Mead[16] to determine the contribution of the external sources to the magnetic field interior to the magnetosphere. They used a centered dipole approximation with an equatorial field strength of 31,000 gammas and assumed impact of the solar

plasma normal to the dipole axis. Satisfying the boundary condition of zero normal component of the net magnetic field and assuming a curl free magnetic region interior to the magnetosphere leads to the following values for the external sources:

$$G_1^{\,o} = -0.277\ (R_e/R_b)^3 \text{ gauss equals } 27.7 \text{ gammas at } R_b = 10\ R_e$$

$$G_2^{\,1} = 0.108\ (R_e/R_b)^4 \text{ gauss equals } -1.1 \text{ gamma at } R_b = 10\ R_e$$

At altitudes greater than 5 R_e the contribution is large. For example at 10 earth radii the external field contributes 46 gammas while the internal field contributes only 31 gammas. At 5 R_e the contribution of the external field is reduced to 37 gammas while the internal field is increased to 248 gammas. We see that in the noon meridian the distortion is large, approximately 15% at a distance of 5 R_e but on the midnight meridian the situation is vastly different. Satellites are presently investigating this particular region of space and theoretical predictions and experimental evidence indicate that the earth's magnetic field may trail out far into interplanetary space well beyond the orbit of the moon in a fashion analogous to the structure of cometary tails in interplanetary space. In conclusion, for accuracies of the geomagnetic field representation of several percent one must restrict altitudes at present to less than about 4 R_e and include external sources for greater altitudes.

Interplanetary Field Representation

On the assumption that

(1) the efflux of solar plasma from the sun is radially outward at velocity V_s

(2) the rate of solar rotation is 2.9×10^{-6} radians per second ($=\Omega$)

(3) assuming a photospheric magnetic field strength given by B_o it is possible, following Parker[17], to predict the strength of the interplanetary magnetic field as

$$B = B_o \left(\frac{a}{r}\right)^2 \sqrt{1+\left(\frac{r\Omega}{V_s}\right)^2} \qquad (2)$$

where a = radius of sun

r = heliocentric distance

This theoretical model of the interplanetary field shows a characteristic geometrical configuration in interplanetary space which resembles the classical Archimedean spiral in the ecliptic plane. A representation of this spiral structure in the interplanetary field is shown in Figure 12. The fixed rotation rate of the sun and high plasma velocity combine to drag out the lines of magnetic force by the highly ionized gases and leads to these characteristic structures. In Figure 13 the theoretical angle, as measured in the plane of the ecliptic, which the field makes with a radial line to the sun

is shown as a function of plasma velocity. It should be noted that the particle density has no bearing on the direction of the interplanetary magnetic field strength nor its magnitude. It is seen that the theoretical angle ϕ is approximately 135^{o} near the orbit of the earth.

Direct measurements of the interplanetary magnetic field have been performed from the IMP-1 satellite. These measurements indicate a striking consistency with the theoretical model just discussed. A sample of the magnetic field measurement in interplanetary space obtained on the IMP-1 satellite is shown in Figure 14. It is seen that the magnitude is approximately 5 gammas and that the field is reasonably near the plane of the ecliptic and approximately at the azimuthal angle theoretically predicted. This indicates, by extrapolation to the surface of the sun, that field magnitudes on the order of several gauss at least are present. It also means that for space probes going inward toward the sun a general increase in the magnetic field strength should be observed. Unfortunantly the one satellite carrying magnetometers to date which has investigated the region of space towards the sun, Mariner II, was contaminated by spacecraft magnetic fields and did not allow accurate measurements to be performed.[18]

Simulation of Magnetic Fields in Space

The preceeding discussion has summarized our present knowledge of magnetic fields in space and presented a foundation upon which we can base out requirements for simulation of

such magnetic fields. The most common method employed in the past has been to utilize circular coils of wire carrying currents to create a magnetic field whose magnitude and direction can be controlled. The first coil system developed was due to Ampere and consisted of a single coil as illustrated in Figure 15. In this case the axial component of the magnetic field is given by

$$H_Z(0,0,Z)=\frac{i}{2}\,\frac{A^2}{\left[(Z-Z_0)^2+A^2\right]^{3/2}} \qquad (3)$$

Two such coil systems placed symmetically with respect to the origin at $\pm$ B give

$$H_Z(0,0,Z)=\frac{iA^2}{2}\left\{\frac{1}{\left[(Z-B)^2+A^2\right]^{3/2}}+\frac{1}{\left[(Z+B)^2+A^2\right]^{3/2}}\right\} \qquad (4)$$

In order to optimize the two coil configuration it is desirable to have a maximum field on the Z axis for a minimum current. This is obtained analytically by differentiating the above formulation, setting it equal to 0 and solving for the various values permitted:

$$\left.\frac{\partial H_z}{\partial z}\right|_{0,0,z} = 0 \qquad (5)$$

In addition, in order to provide a maximally homogeneous magnetic field one would require a minimum gradient of the actual component of the magnetic field. This is determined by setting the second derivative of the field with respect to Z equal to 0 as shown below

$$\left.\frac{\partial^2 H_z}{\partial z^2}\right|_{0,0,z} = 0 \qquad (6)$$

Now clearly at Z equals 0 the field is a maximum regardless of the value of B as long as the location of the two coils is chosen to be symmetric. However, in order that the gradient to be a minimum then the final result of formula (6) is that $4B^2 = A^2$ or that $A = 2B$. This optimum coil configuration utilizing

two coils was developed by Helmholtz many years ago and has become a standard reference in the simulation of magnetic fields in space.

Maximum uniform magnetic fields utilizing multiple sets of coil pairs rely on these two principles:

1. That pairs of coils symmetrically located with respect to the orgin give maximum fields and
2. Minimum gradients if appropriately positioned (which can be determined by analytical investigations).

One can introduce four coils with different numbers of windings on each pair of coils or vary the distances and/or size of radii. In general the homogeneity of the magnetic field is the most important goal since symmetry quite easily achieves the maximum field. Indeed a figure of merit can be defined which measures the degree of homogeneity as:

$$100\left[1-\frac{H(x,y,z)}{H(0,0,0)}\right]=\%\ \text{Homogeneity} \qquad (7)$$

Now the Helmholtz coil provides a homogeneity of $\pm$ 1% along the axis if the absolute value of Z is less than .32 A. It has a maximum error of $\pm$ 1% off the axis if the absolute value of $\sqrt{X^2+Y^2}$ is less than .38 A. It is seen that the region of space homogenous in magnitude to 1% is roughly an oblate

spheroid whose dimensions of principal axes are given by .32A, .38A, .38A.

Now the earth's magnetic field is approximately 50,000 gammas and one percent of this is 500 gammas so that for interplanetary work one needs a uniformity much better than one percent. In order to provide a homogeneity of one gamma over a working region of space implies a requirement of homogeneity of .001%. For a Helmholtz coil this implies a very small region of space and a large coil radius. Indeed, for an homogeneity of 0.1% the dimensions of the region of space are approximately one half the dimensions for 1% accuracy, being .16A, .2A and .2A. For values of .001% the dimensions are .04A, .05A and .05A, so that if the radius of the coils is 25 feet then one has a sphere of approximately 1 foot radius in which the field is homogeneous to 1 gamma. Clearly the practical liminations of constructing such large coil systems requires a re-evaluation of the utility of the very simple Helmholtz configuration. It is found that by adding more coils but using the same principles governing the development of the Helmholtz system one can rapidly improve upon the situation for the practical development of coil systems.

An intriguing possibility but one which has not proven successful in practical applications is available in what is referred to as a "sine winding" coil system. In this geometry the density of turns per unit length actually is held constant

while the coil is continuously wound on the surface of a sphere. This provides a completely uniform magnetic field interior to the spherical surface. Unfortunately such a configuration is not reasonably practical when consideration of access to the coil system is made.

The general approach is to develop hybrid coil systems utilizing multiple pairs of coils and employ analytical procedures to determine optimum coil constants and configurations. One begins by using circular coordinates and expressing the potential V in cylindrical harmonics and then determining the appropriate turns and current values.[19] The important considerations in the development of such coil systems are:

1. The difficulty in implementing the coil manufacture, which has lead to consideration in some instances of square coil systems,
2. Current stability and current ratios required, which has lead to constant current but separate turns ratios for coil pairs rather then attempting to develop precise current dividers utilizing resistive ratios only;
3. The accessibility for various geometries, which has lead to the development of cubic and square coil systems and
4. The analytical difficulties in developing optimum coil systems, which have lead students of coil geometries to consider mainly equal amp terms or sets of coils

which lie on the surface of a sphere but at different distances along the axis of the system.

A summary of some existing coil systems and their figure of merits is shown in Table I.

Summary of Some Existing Optimum Coil Systems

Name	Dimensions	volume of Homogeneity (0.1%)	Turns ratio
Circular Helmholtz	b = 0.5a	0.9%	1:1
Fanselau[20]		14%	equal amp turns
Braunbek[21]		22%	" "
McKeehan[22]		22%	on surface of sphere
Square Helmholtz[19]	b = 0.55a	1%	1:1
4 Coil Cubic[19]	b = ± .33a, ±a	0.8%	46:43:43:46
5 Coil Cubic[19]	b = 0, ± .5a, ±a	2.2%	134:44:66:44:134

TABLE I

Presently the Goddard Space Flight Center is fabricating a 25 foot Braunbek coil system in which three separate sets of such coils are employed for three axis cancellation of the earth's magnetic field. The specific parameters of the GSFC facility are;

1. the diameter of the smaller coil is .76388 of the larger,
2. the separation of the smaller is .84565 of the larger

diameter, and

3. the separation of the larger coils is .27803 of the larger diameter, and
4. The real diameter of the coil systems are:
   (a) the vertical is 22 feet,
   (b) the horizonal east-west magnetically oriented is 18 feet and
   (c) the horizonal north-south magnetic is 16 feet.

The orientation of the geomagnetic field at the Goddard facility is such that a larger coil system is required for the vertical component since it is the largest in magnitude, while the remaining coil systems are chosen to be compatible with practical implementation of an inter laced set of such coils.

In Figure 16 is shown a picture of a model of the GSFC coil system. The coil constant is 15.4 gammas per milliamp and there are 36 turns of number 6 copper wire on each coil. The performance of the Braunbek coil system is seen, by review of the characteristics of Table I, to be equivalent to a McKeehan and to have the additional merit that equal amp turns on each coil system are required, whereas the other requires different currents in each of the coils. The measured performance of the Goddard facility provides a homogeneity of .001% in a 1 meter diameter sphere with an accuracy of $\pm$ 0.5 gamma and a resolution of 0.1 gamma.

An important aspect of such coil systems is that they be capable of being servo controlled to simulate a stationary weak magnetic field in spite of the fact that the earth's magnetic field varies as a function of time. A secondary set of coils is associated with this coil facility and is used to monitor the variations of the geomagnetic field. The stability of the coil system is approximately 1/2 to 1 gamma and the cancellation of the earth's magnetic field can thus be automatically controlled. The Goddard facility is not yet completely operational although sensible measurements have been made utilizing the coil systems. The completed system is scheduled for March 1965. As such it will be the largest and most accurate facility in the world.

Spacecraft Applications

The most important application of any coil system is its ability to simulate magnetic fields which represent those to be measured in space for calibration of magnetometer sensors. A secondary objective is to permit the mapping magnetically of the inherent magnetic properties of spacecraft and spacecraft sub-systems whose magnetic fields may yield adverse effects on the data collected. The following paragraphs summarize briefly the specific applications of the knowledge of the earth's magnetic field and its interaction with satellites which have developed over the past several years.

Vanguard I - Spin Decay

The Vanguard I satellite provided a unique example for investigation of the electro magnetic interaction of a spin stabilized satellite with the earth's magnetic field over a long time scale. The basic physics involved is based upon the fact that a rotating sphere in a magnetic field will induce eddy currents in a fashion such as to generate currents whose magnetic fields not only oppose the spin, but whose currents lead to dissipation of Kinetic energy. On the assumption that the electro magnetic readjustments, as the spin axis changes inclination with respect to the magnetic field, occur at a rate much greater than the mechanical readjustments, the theoretical development and explanation of the Vanguard I spin rate decay can be understood. The first investigation was conducted by J. P. Vinti assuming a spherical shell of uniform conductivity and non-magnetic material. The characteristic summary of the results is that the induced eddy currents create a torque on the spinning satellite proportional to the inertial moment of the satellite, and the angular spin rate and the magnetic field strength squared as shown in the formulae below:

$$\overrightarrow{\text{Torque}} \propto I(\vec{\omega} \times \vec{B}) \times \vec{B} \qquad (8)$$

where I is the angular moment of inertia
ω is the angular velocity
$\vec{B}$ is the magnetic field vector

The net result of the torque can be separated into a spin decay which is proportional to the angular spin rate and its product with the magnetic field perpendicular to the spin rate as shown in the following formula:

$$L(\text{decay}) \alpha \omega B_{\perp}^{2} \quad (9)$$

Similarly the precession torque is

$$L(\text{precession}) \alpha \omega B_{\perp} B_{\parallel}$$

The Vanguard I satellite was launched March 17, 1958 into an orbit with elevations between 650 to 3,900 Km at which the earth's magnetic field was approximately 40 to 30 thousand gammas. The spin decay studies indicated the satellite slowed down from an initial rate of 3.0 rps to 0.05 rps in 2.5 years.[24] These measurements were performed by investigation of the periodic fading of radio signals associated with the antenna pattern of the satellite. The first anomaly was detected in December 1958 and a rapid evaluation of theoretical models which go back to Hans Hertz in 1896 indicated that classical EM theory could explain the observed anomaly.

Injun III Passive Magnetic Orientation

The motions of charged particles trapped in the earth's magnetic field are generally helical spirals about field lines with associated drift of electrons east and protons west due

to the spatial gradient of the earth's magnetic field. The particles "bounce" back and forth along a line of force between their "mirror" points. The angle that the spiral makes with the field lines is called the pitch angle and and is an important parameter to be measured in charged particle investigations in space. Since it is known that the first adiabatic invariant of particle motion is preserved then measuring the pitch angle distribution of the particles at a point in space predicts the particle flux characteristics along that line of force. The variation in pitch angle is shown by the following formula in which B_o is the field strength when $\alpha = 0^o$ and B_m is the field strength at the mirror point when $\alpha = 90^o$.

$$B_o = B_m \sin^2 \alpha_{90^\circ}$$

and in general

$$\sin^2 \alpha = \frac{B_o}{B} \qquad (10)$$

In order to separate by direct detector analysis the pitch angle distribution requires unique instrumentation. An ingeneous suggestion has resolved this difficulty by placing a bar magnetic [25] in the spin stabilizated spacecraft Injun III so that the satellite spin axis becomes parallel to the local magnetic field. Recalling the results of the previous discussion on Vanguard I, it is found that both the decay and the precession torques are

zero for perfect alignment of the magnetic vector and spin vector of the satellite. In the Injun III satellite an Alnico-V magnet 22 inches long and 1 inch square was employed and permalloy rods perpendicular to the spin axes were employed to damp the periodic motion induced by the variable aspect to the earth's magnetic field. The Injun III satellite was launched December 13, 1962 and achieved an apogee of 2787 Km. and a perigee of 237 Km. The natural period of this satellite was approximately two minutes and the satellite damped to being almost perfectly aligned with the earth's magnetic field in approximately three days. The success of this particular passive orientation device was checked by onboard magnetometers measuring the magnetic field perpendicular to the spin axis of the satellite.

Tiros-Active Attitude Control System

The Tiros wheel satellite, number 9, will be launched into a circular orbit of 13,000 Km with a unique active attitude control system utilizing the principles already discussed. It will be placed into a near polar orbit with the spin axis perpendicular to the orbital plane and sun synchronized so that the precession of the orbital plane due to the earth's equatorial bulge will maintain the satellite in a solar orientation so that a constant illumination of the observed earth's surface is maintained. The magnetic aspect control system (MASC) will keep the spin within its proper limits and the quarter orbit magnetic attitude control system (QOMAC) will keep

the spin axis perpendicular to the orbital plane. These systems are illustrated in figure 17 with respect to orientation to the satellite spin axis

The need for such current carrying coil systems was not recognized until after Tiros I.[26] On successive Tiros, numbers II through VIII, the magnetic attitude control system was utilized mainly to provide proper cancellation of the satellites magnetic field so that spin torques on the satellite were negligible. It is possible to alter the polarity of the spacecraft dipole moment by these coil systems and indeed the magnetic properties of the satellite are planned to be cancelled continously by these attitude systems.

SUMMARY

The above discussion has been very brief but illustrates the utilization of the earth's magnetic field in attitude control systems going from strictly interaction to highly sophisticated computer programmed active attitude systems. The necessity for verifying the operation of such systems is clear and the utilization of large coil facilities for attitude studies such as that being fabricated at GSFC is clearly indicated.

References

1. Beard, D. B., The interaction of the terrestrial magnetic field with the solar corpuscular radiation, J. Geophys. Res., 65, 3559-3568, 1960.

2. Heppner, J. P., N. F. Ness, T. L. Skillman, and C. S. Scearce, Explorer X magnetic field measurements, J. Geophys. Res., 68, 1-46, 1963.

3. Van Allen, J. A., Dynamics, composition and origin of the geo-trapped radiation, in Space Science edited by D. P. Legalley, John Wiley and Sons, New York-London, 1963.

4. OBrien, B. J., Review of Studies of Trapped Radiation with Satellite-Borne Apparatus, Space Science Revs., 1, 415-484, 1963.

5. Ness, N. F., C. S. Scearce, J. B. Seek, Initial Results of the IMP-1 Magnetic Field Experiment, J. Geophys. Res., 69, 3531-3569 1964.

6. Chapman, S. and Ferraro, V. C. A., A new theory on magnetic storms, Terr. Mag. and Atmos. Elec., 36, 77-97, 171-186, 1931; 37, 147-156, 421-429, 1932; 38, 79-96, 1933.

7. Gold, T., The Motions in the Magnetosphere of the Earth, J. Geophys. Res., 64, 1219-1224, 1959.

8. Snyder, C. W. and M. Neugebauer, Interplanetary solar wind measurements by Mariner II, Space Res., IV, to appear 1964.

9. Bonetti, A., H. S. Bridge, A. J. Lazarus, B. Rossi, and F. Scherb, Explorer X plasma measurements, J. Geophys. Res. , 68, 4017-4063, 1963.

10. Bridge, H., A. Egidi, A. Lazarus, E. Lyon and L. Jacobson Preliminary results of plasma measurements on IMP-A, COSPAR presentation, Florence, Italy, 1964.

11. Kellogg, P. J., Flow of plasma around the earth, J. Geophys. Res., 67, 3805-3811, 1962.

Axford, W. I., The interaction between the solar wind and the earth's magnetosphere, J. Geophys. Res., 67, 3791-3796, 1962.

12. Lees, L., Interaction between the solar plasma wind and the geomagnetic cavity, N. Y. meeting of AIAA, January, 1964. Preprint 64-88.

13. Ness, N. F. and J. M. Wilcox, Solar Origin of the Interplanetary Magnetic Field, Phys. Rev. Letters 13 (15), 461-464, 1964.

14. Chapman, S. and J. Bartels, Geomagnetism, Oxford, 1940

15. Heuring, F. T., The Analytic Description of the Geomagnetic Field at Satellite Altitudes, J. Geophys. Res., 69, 4959-4968, 1964.

16. Mead, G. D. and D. B. Beard, Shape of the geomagnetic field solar wind boundary, J. Geophys. Res., 69, 1169-1180, 1964.

Mead, G. D. Deformation of the geomagnetic field by the solar wind, J. Geophys. Res., 69, 1181-1195, 1964.

17. Parker, E. N., Dynamics of the interplanetary gas and magnetic fields, Astrophys. J., 128, 667-676, 1958.

18. Smith, E. J., P. J. Coleman, and L. Davis, Interplanetary magnetic field measurements with Mariner 2, paper presented at JPL Symp. Solar Wind, Calif. Inst. Tech., Padadena, Calif., April 1-4, 1964, to be published, 1964.

19. Warburton, F. W., Design of Coil Systems for Magnetic Field Control at the Naval Ordnance Laboratory, NAVORD Report 3768, 1955.

20. Fanselan, G. Die Erzengung Weitgehend Homogener Magnetfelder durch Kreisstrome,
Zeits. Phys., 54,260-269, 1929.

21. Braunbek, W., Die Erzeugung Weitgehend Homogener Magnetic-felder durch Kresstrome,
Zeits., Phys., 88, 399-402, 1934

22. McKeehan, L. W., Combinations of circular currents for producing uniform magnetic fields, Rev. Sci. Instr., 7, 150-153, 1936.

23. Vinti, J. P., Theory of the Spin of a Conducting Satellite in the Magnetic Field of the Earth, Aberdeen Ballistic Research Laboratory Report 1020, 1957.

24. Arendt, P. R., Anomalies of the Geomagnetic Retardation of the Spin of Satellite Vanguard I (1958 Beta), ARS Journal 31-3, 286-289, 1961.

25. OBrien, B. J., C. D. Laughlin and D. A. Gurnett, High-Latitude Geophysical Studies with Satellite Injun 3, 1. Description of the Satellite, J. Geophys. Res., 69, 1-12, 1964.

26. Grasshoff, L. H., Eddy Current Torgue Compensation in a Spin Stabilized Earth Satellite, ARS Journal 31-3, 290-293, 1961.

LIST OF FIGURES

4. Results of the Explorer X measurements of the geomagnetic field from 4 to 12.5 R_e. The observations are indicated by solid dots connected by straight line segments, the theoretical values indicated by solid lines and interpreted fit assuming a constant field indicated by the dashed line.
5. Results of the traversal of the magnetosphere boundary by IMP-I on inbound orbit pass No. 1. Observed values are indicated by open and closed circles connected by straight line segments as provided by both the rubidium vapor magnetometer and the fluxgate magnetometers carried onboard the satellite. The dashed curves represent the theoretical magnetic field extrapolated from terrestrial surface measurements. At these distances the only contributing factor in the multipole expansion of the earth's field is the dipole moment of the earth. The abrupt transition at 10.7 R_e identified as the boundary of the magnetosphere, the magnetopause .
6. Naive representation of the interaction of the solar plasma with the geomagnetic field. Direct impact of the plasma with the magnetic field is shown as being specularly reflected from the geomagnetic boundary. The distance to the boundary at the subsolar point is given by:

$$R_m = R_e \left[\frac{B_o^2}{4\pi\, mn\, V_s^2} \right]^{1/6}$$

where R_e is the radius of the earth, B_o is the equatorial magnetic field strength and V_s the velocity of the solar plasma with density n p/cm^3.

7. Theoretical size of the magnetosphere at the subsolar point assuming normal impact of the solar plasma on the geomagnetic field. For a magnetosphere of size 10.7 R_e at the stagnation point, and assumed velocity of 400 km/sec the deduced equivalent plasma density is 2 protons per cubic centimeter.

8. Summary pre-IMP-1 illustration of the confined geomagnetic field of the earth and the location of the radiation belts. The flow of solar plasma is taken to be directly from the sun and the trace of the Explorer X trajectory is shown on the magnetic meridian plane.

9. The results of the magnetic field experiment carried on the IMP-I spacecraft from orbit No. 15, January 21, 1964. These data illustrate the outbound traversal of the magnetosphere boundary at 15.7 R_e and the collisionless magnetohydrodynamic shock wave at 22.7 R_e, with a possible precurser occurring at 24.5 R_e.

10. Alfven magnetohydrodynamic phase velocity of wave propagation as a function of magnetic field strength and plasma density. Representative values for the interplanetary medium are chosen in this diagram.

11. Comparison of the observed positions of the boundary of the magnetosphere and shock wave as shown by solid dots with the theoretical positions according to the computations of Spreiter and Jones (1963) adjusted for a different gas dynamic specific heat capacity ratio. Very good agreement is obtained with this modification of their treatment and an aberration by 5^{o} to accommodate the heliocentric orbital motion of the earth around the sun. The distance to the magnetosphere boundary at the subsolar point is 10.25 R_e and the distance to the shock wave boundary is 13.4 R_e.

12. Schematic illustration of the spiral interplanetary magnetic field as obtained by assuming a uniformly expanding, infinitely conducting solar corona. The topology of the interplanetary magnetic field changes significantly as the velocity of the plasma increases. At high velocities the field lines are radially directed, paralleling the flow field from the sun, while for very low velocities the field lines are tightly wound in a Archemedian spiral configuration as shown on the left hand side.

13. Theoretical direction of the interplanetary magnetic field as measured by the azimuthal angle ϕ in the plane of the ecliptic as a function of the solar wind velocity V_s.

14. Representative measurements of the interplanetary magnetic field from IMP-I during orbit 15, January 22, 1964. These data follow immediately after those of Figure 9 and indicate the characteristic of the interplanetary magnetic field magnitude and variability of the direction.

15. Geometry and relative scale of the Ampere coil and Helmholtz coil configurations utilized to nullify the earth's magnetic field in space simulation. The Z axis of the coil system is normal to the plane of the coils.

16. Model of the Goddard Space Flight Center, Magnetic Fields component test facility located adjacent to the laboratory in Greenbelt, Md. This large scale coil facility will be utilized for calibration of magnetometer sensors and mapping of magnetic field properties of spacecraft and subsystems.

17. Schematic illustration of the Tiros wheel satellite geometical configuration of coil systems employed to control the aspect and attitude of the satellite. Electrical currents can flow in either polarity on the coils as indicated under ground computer control.

SATELLITE	INSTRUMENT	RANGE	SENSITIVITY	DISTANCE
SPUTNIK III	TRIAXIAL FLUXGATE	$<6\times10^4$	5%	<1.3
PIONEER I	SEARCH COIL	$<10^3$	1%	3.7-7.0 12.3-14.6
LUNIK I	TRIAXIAL FLUXGATE	<6000	200γ	3-6
EXPLORER VI	SEARCH COIL SOLAR ASPECT	$<2\times10^4$	3%	2-7.5
LUNIK II	TRIAXIAL FLUXGATE	<1500	50γ	3-6
VANGUARD III	PROTON PRECESSION	$10^4-6\times10^4$	4γ	<1.8
PIONEER V	SEARCH COIL	$<10^3$	0.05-5γ	5-9
EXPLORER X	RB VAPOR FLUXGATES	$30-5\times10^3$ ±50	3γ 0.3γ	1.8-7 6-42.6
EXPLORER XII	TRIAXIAL FLUXGATE	±500	10γ	4-13.5
EXPLORER XIV	TRIAXIAL FLUXGATE	±250	5γ	5-16.5
ALOUETTE	IONOSPHERIC SOUNDING	$<6\times10^4$	0.3%	1.17
EXPLORER XV	TRIAXIAL FLUXGATE	±4000	40γ	1.7-4.0

Figure 1

SATELLITE	LAUNCH	INCLINATION	LIFETIME(d)
SPUTNIK III	5-15-58	65°	30
PIONEER I	10-11-58	EARTH IMPACT	1
LUNIK I	1-2-59	SOLAR ORBIT	1
EXPLORER VI	8-7-59	47°	61
LUNIK II	9-12-59	LUNAR IMPACT	33.5 HRS.
VANGUARD III	9-18-59	33°	85
PIONEER V	3-11-60	SOLAR ORBIT	50
EXPLORER X	3-25-61	33°	2.2
EXPLORER XII	8-16-61	33°	112
EXPLORER XIV	10-3-62	33°	300
ALOUETTE	9-29-62	80°	STILL TRANS.
EXPLORER XV	10-27-62	18°	90

Figure 2

STUDIES OF THE INTERPLANETARY MAGNETIC FIELD

SPACECRAFT (LAUNCH)	LIFETIME (DAYS)	REGION	INSTRUMENT	SENSITIVITY	ACCURACY	COMMENTS
PIONEER V (3-11-60)	50	.9-1.0 AU	SEARCH COIL	$\angle 0.1^{\gamma}$	?	COMPONENT $\perp$ TO SPIN AXIS ONLY
EXPLORER X (3-25-61)	2.2	$\angle 47$ R_e	RUBIDIUM, FLUXGATES	$\pm 0.25^{\gamma}$	$\pm 1.0^{\gamma}$	NEVER OUTSIDE EARTHS INFLUENCE
MARINER II (8-26-62)	104	.7-1.0 AU	FLUXGATES	$\pm 0.7^{\gamma}$	?	SPACECRAFT FIELDS, ZEROS UNKNOWN
IMP-A (11-27-63)	STILL OPERATING	$\angle 32$ R_e	RUBIDIUM, FLUXGATES	$\pm .25^{\gamma}$	$\pm .25^{\gamma}$	INITIAL APOGEE TOWARDS SUN

Figure 3

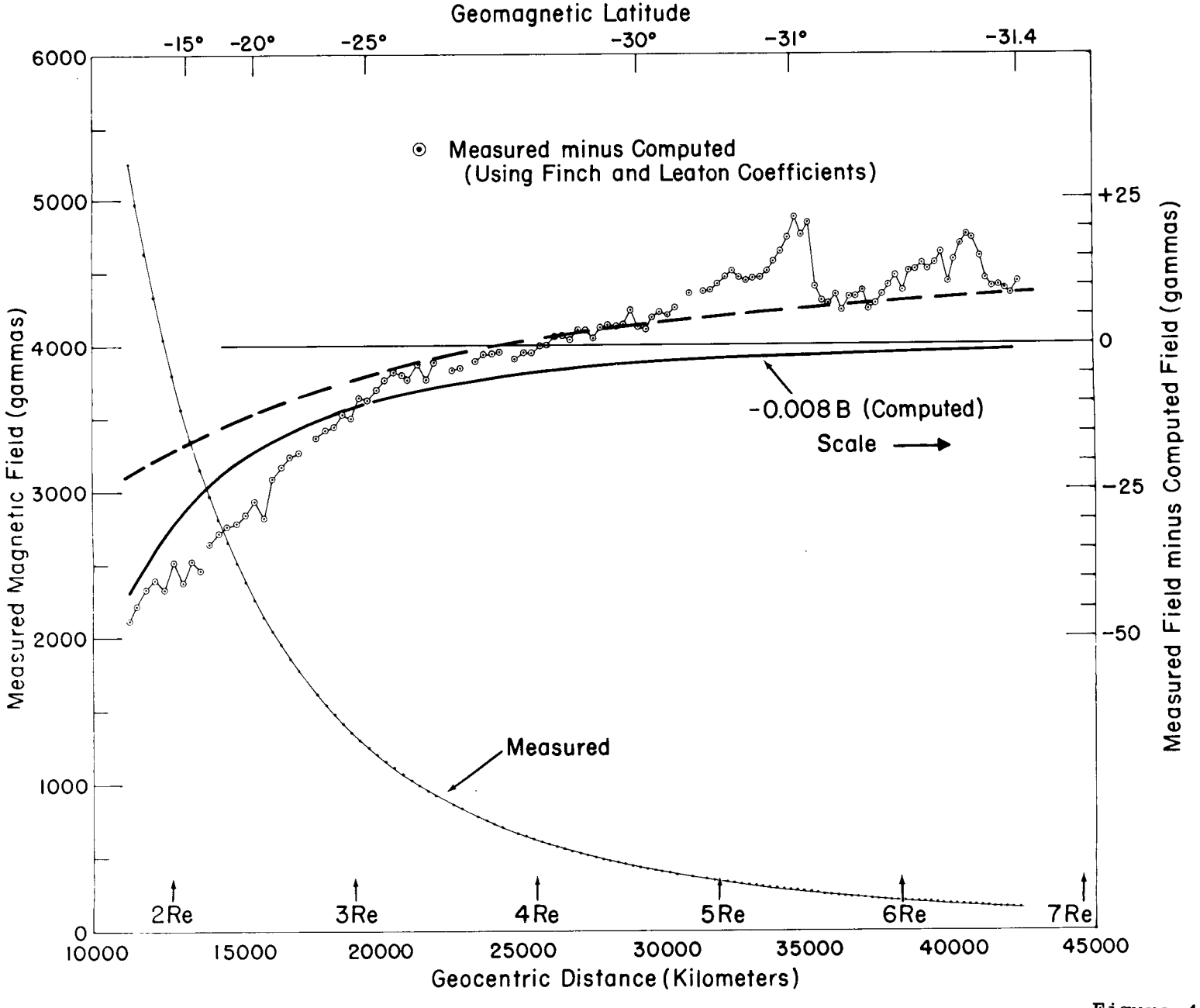
Geomagnetic Latitude
-15°
-20°
-25°
-30°
-31°
-31.4
Measured minus Computed
(Using Finch and Leaton Coefficients)
-0.008 B (Computed)
Scale
Measured
Measured Magnetic Field (gammas)
Measured Field minus Computed Field (gammas)
+25
0
-25
-50
6000
5000
4000
3000
2000
1000
0
2Re
3Re
4Re
5Re
6Re
7Re
10000
15000
20000
25000
30000
35000
40000
45000
Geocentric Distance (Kilometers)

Figure 4

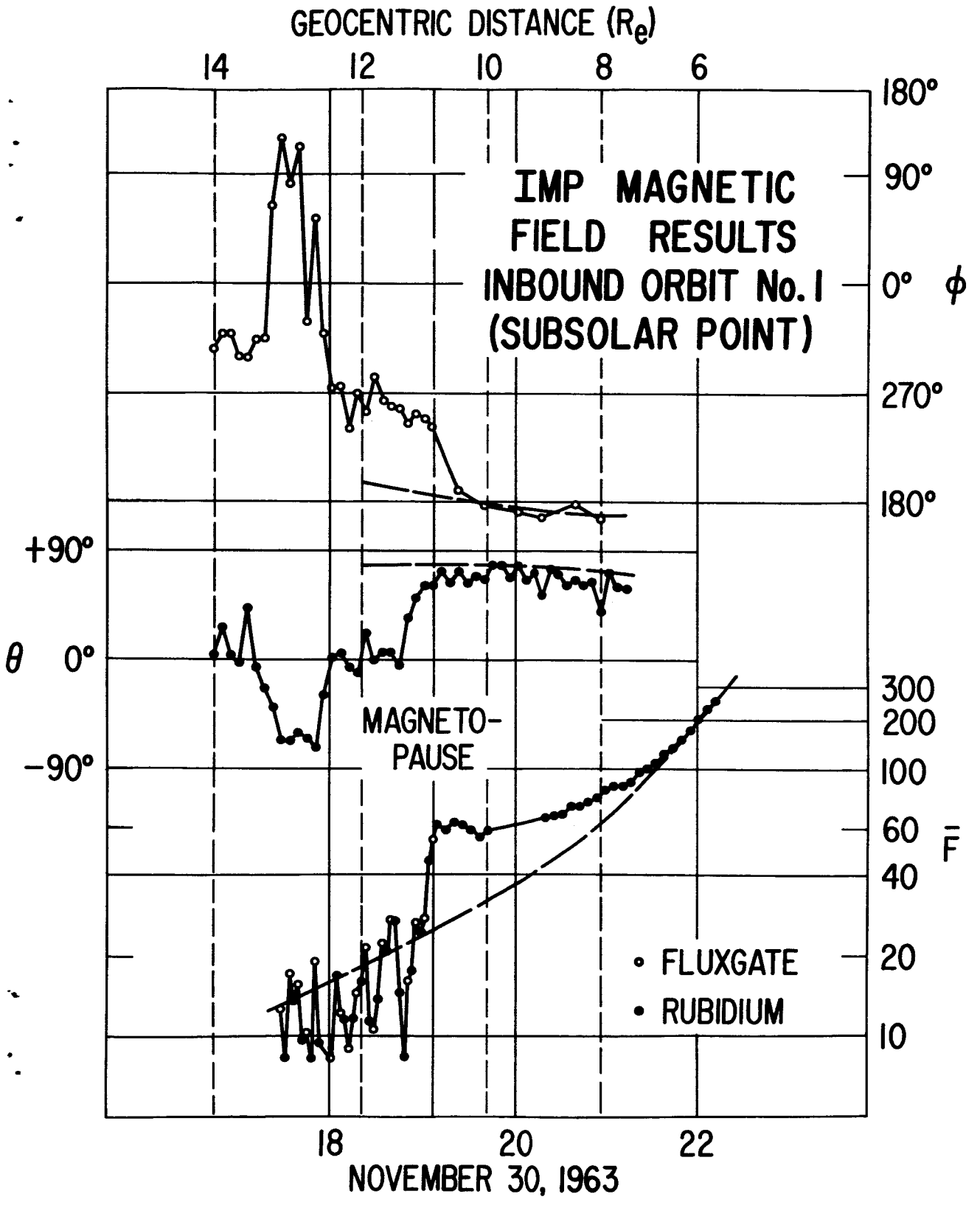
GEOCENTRIC DISTANCE (R_e)
14
12
10
8
6
IMP MAGNETIC
FIELD RESULTS
INBOUND ORBIT No. I
(SUBSOLAR POINT)
180°
90°
0° φ
270°
180°
+90°
θ 0°
−90°
MAGNETO-
PAUSE
300
200
100
60
40
20
10
F
FLUXGATE
RUBIDIUM
18
20
22
NOVEMBER 30, 1963

Figure 5

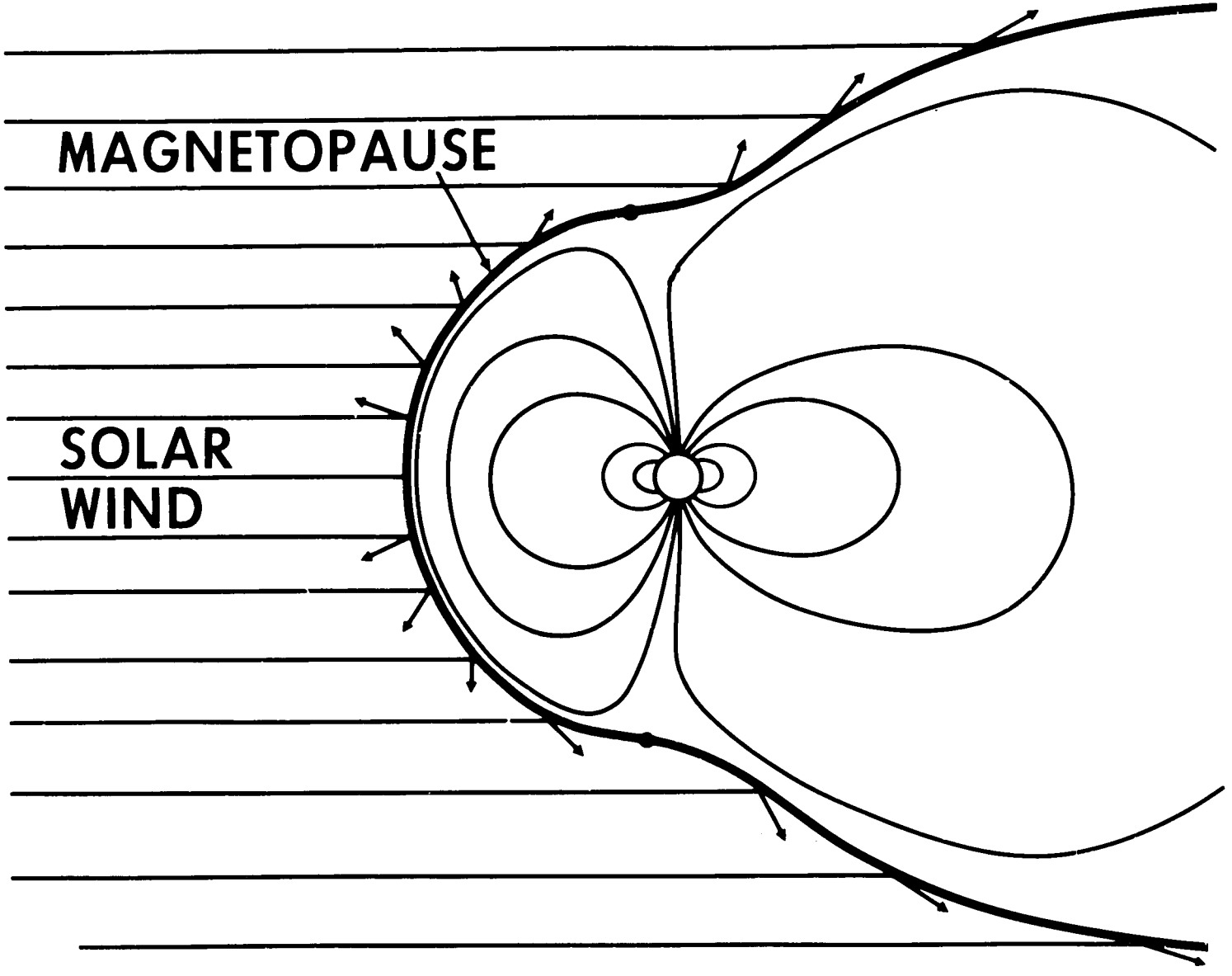

Figure 6

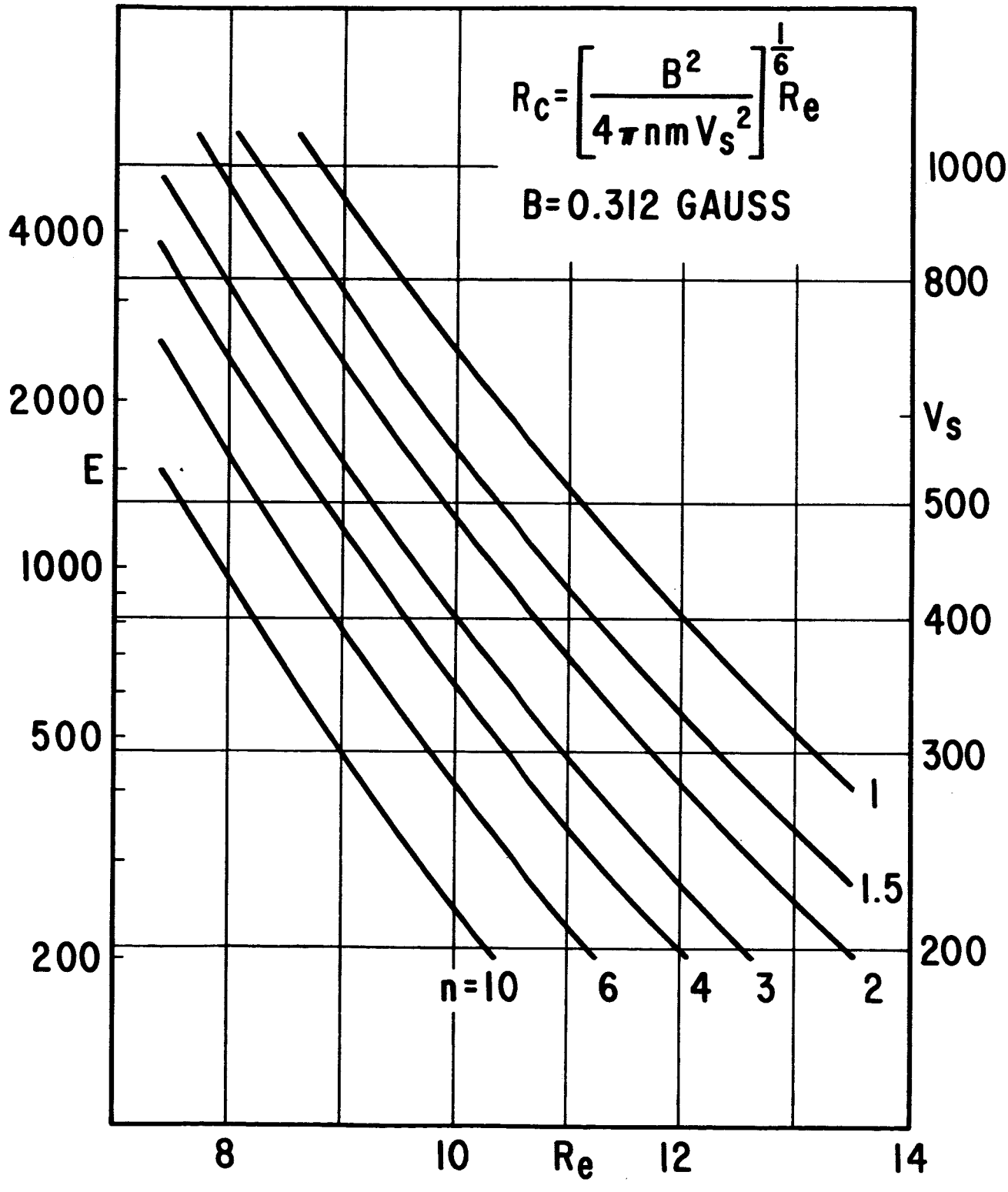
$R_c = \left[\frac{B^2}{4\pi n m V_s^2}\right]^{\frac{1}{6}} R_e$
B=0.312 GAUSS
4000
2000
E
1000
500
200
1000
800
V_s
500
400
300
200
1
1.5
2
3
4
6
n=10
8
10
R_e
12
14

Figure 7

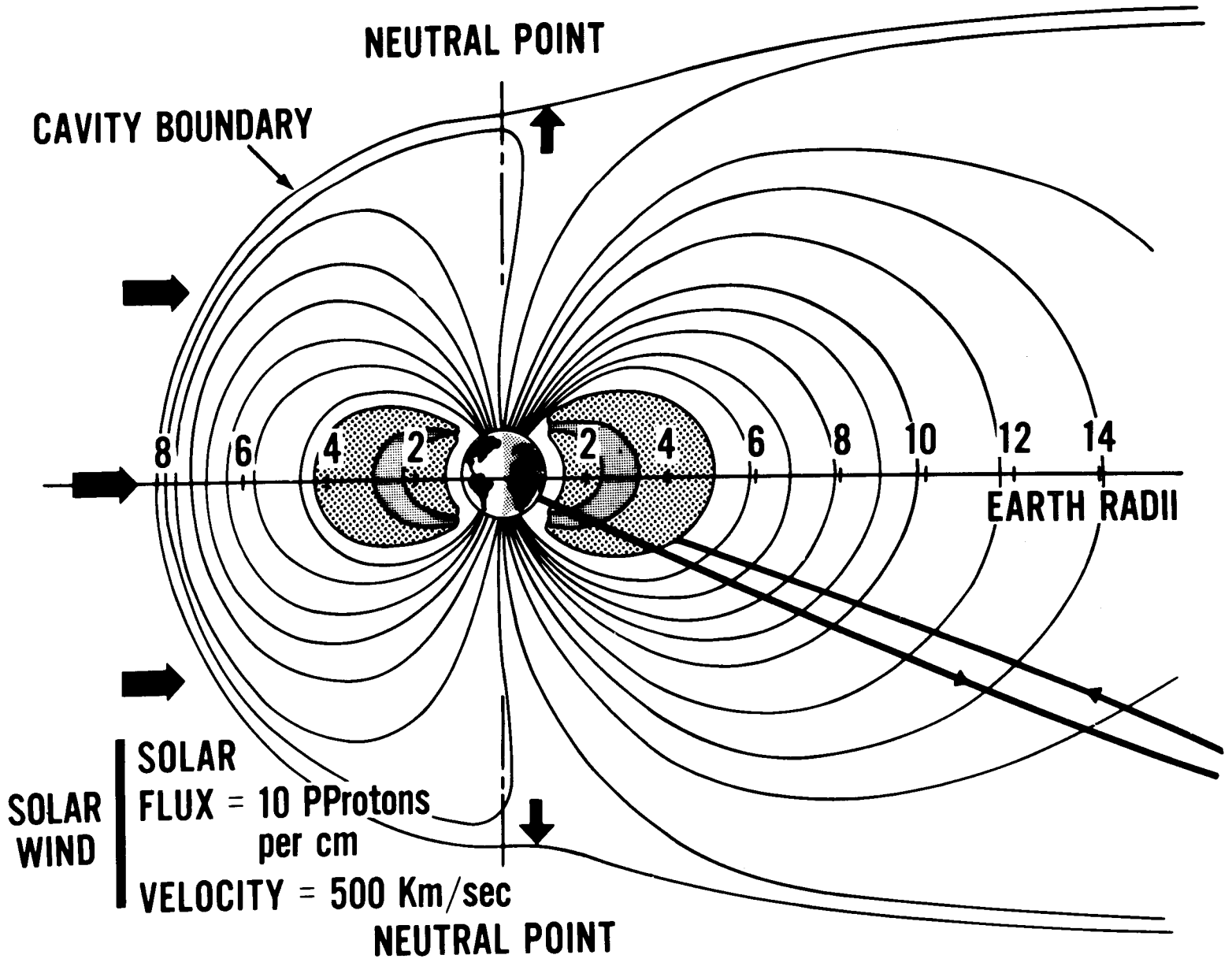
NEUTRAL POINT
CAVITY BOUNDARY
8
6
4
2
2
4
6
8
10
12
14
EARTH RADII
SOLAR WIND
SOLAR
FLUX = 10 PProtons per cm
VELOCITY = 500 Km/sec
NEUTRAL POINT

Figure 8

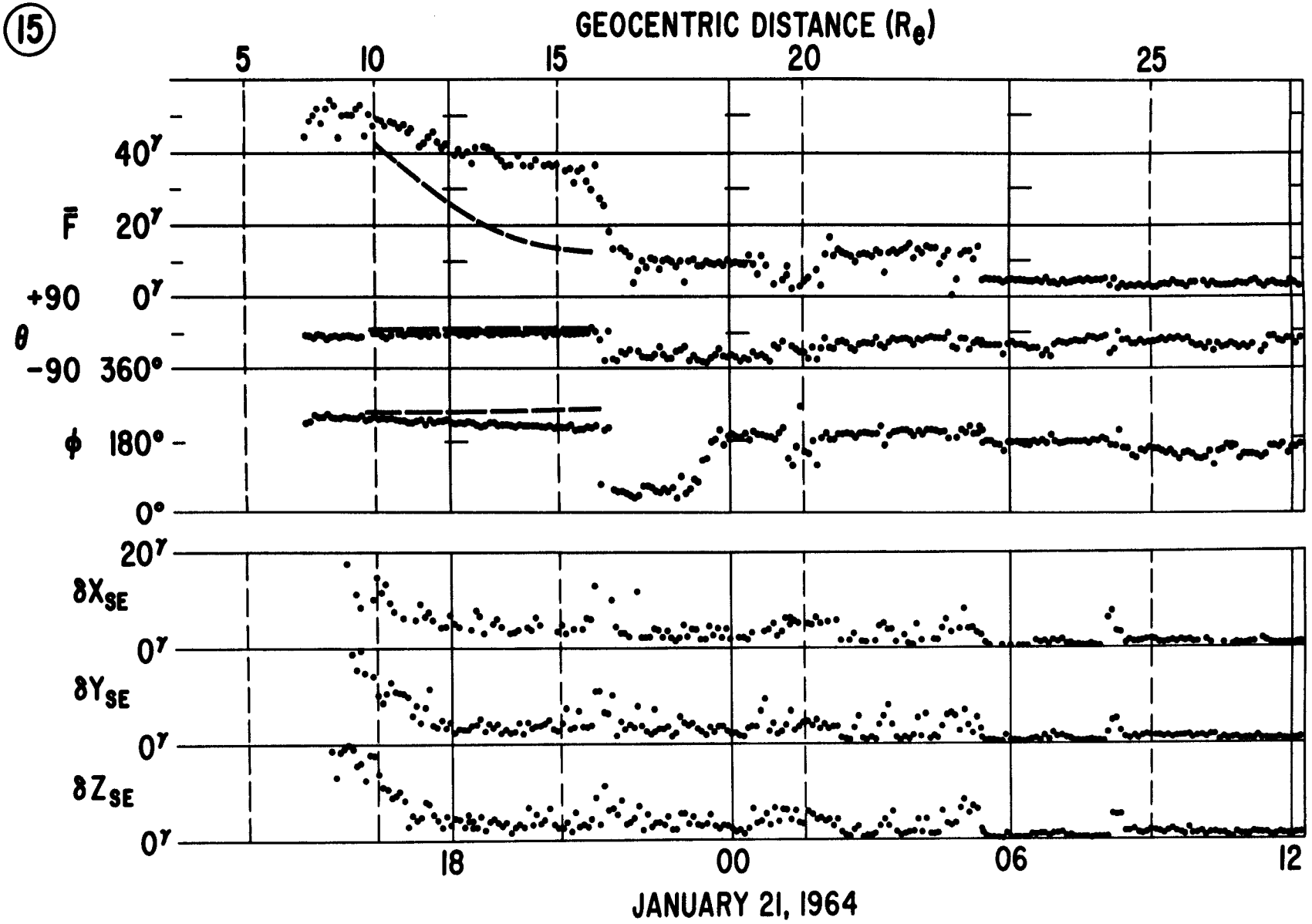
15
GEOCENTRIC DISTANCE (R_e)
5
10
15
20
25
40γ
F̄ 20γ
0γ
+90
θ
-90 360°
φ 180°
0°
20γ
δX_SE
0γ
δY_SE
0γ
δZ_SE
0γ
18
00
06
12
JANUARY 21, 1964

Figure 9

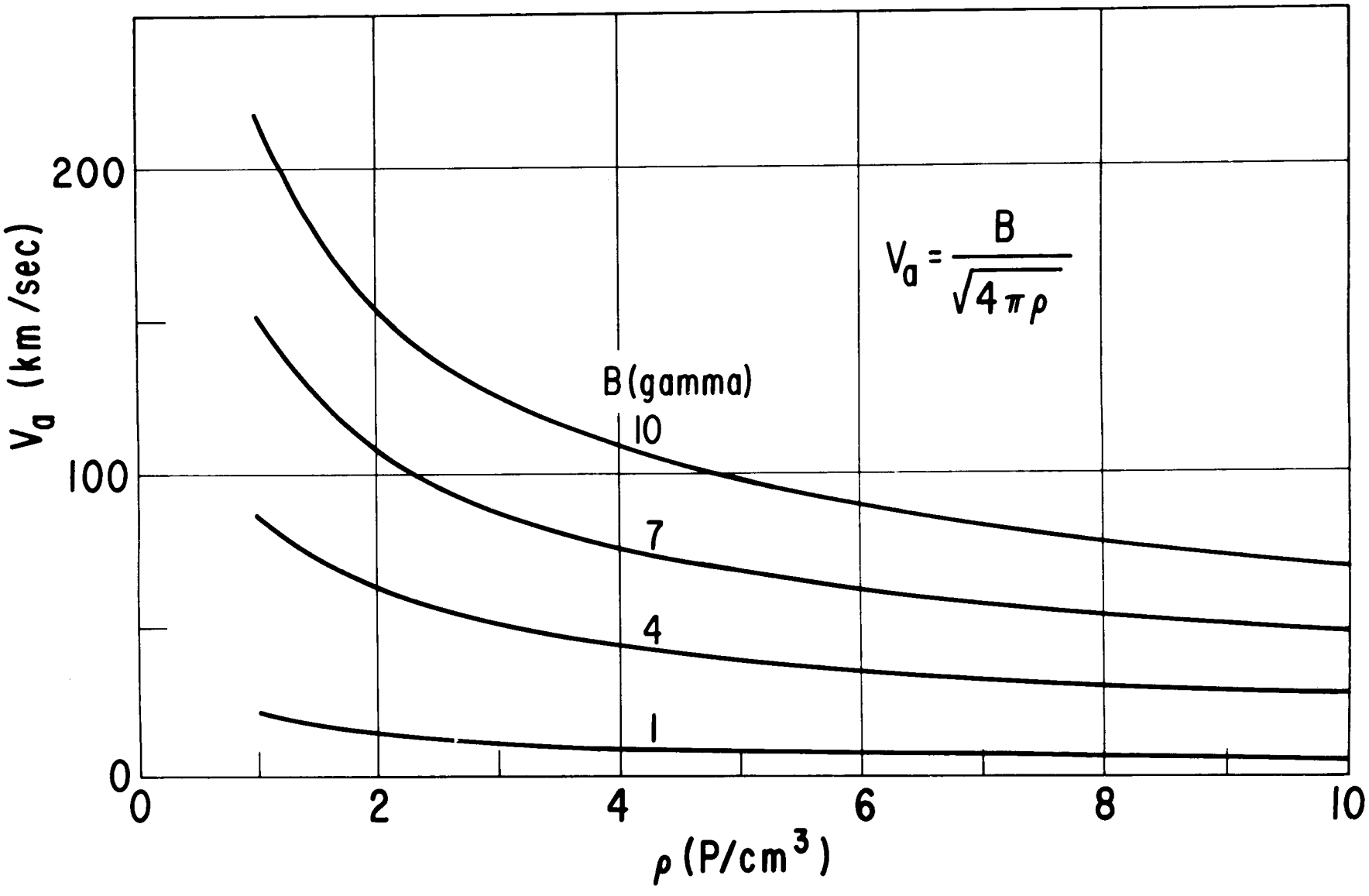
200
100
0
V_a (km/sec)
$V_a = \frac{B}{\sqrt{4\pi\rho}}$
B(gamma)
10
7
4
1
0
2
4
6
8
10
ρ (P/cm^3)

Figure 10

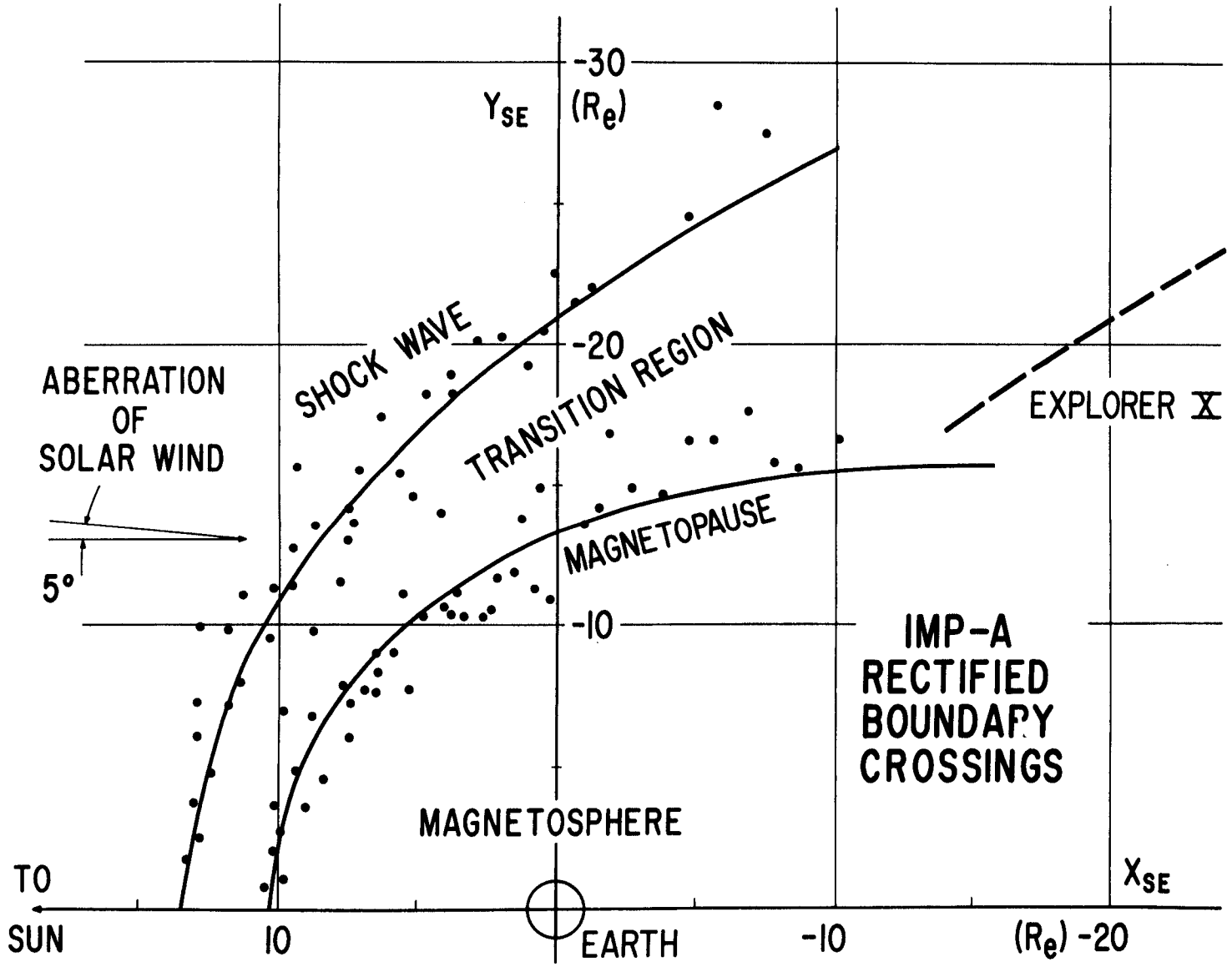
-30
Y_{SE} (R_e)
-20
-10
SHOCK WAVE
TRANSITION REGION
MAGNETOPAUSE
ABERRATION
OF
SOLAR WIND
5°
EXPLORER X
IMP-A
RECTIFIED
BOUNDARY
CROSSINGS
MAGNETOSPHERE
TO
SUN
10
EARTH
-10
(R_e) -20
X_{SE}

Figure 11

THEORETICAL BENDING OF SOLAR WIND MAGNETIC FIELD LINES CAUSED BY SUN'S ROTATION (VIEWED FROM ABOVE THE NORTH POLE)

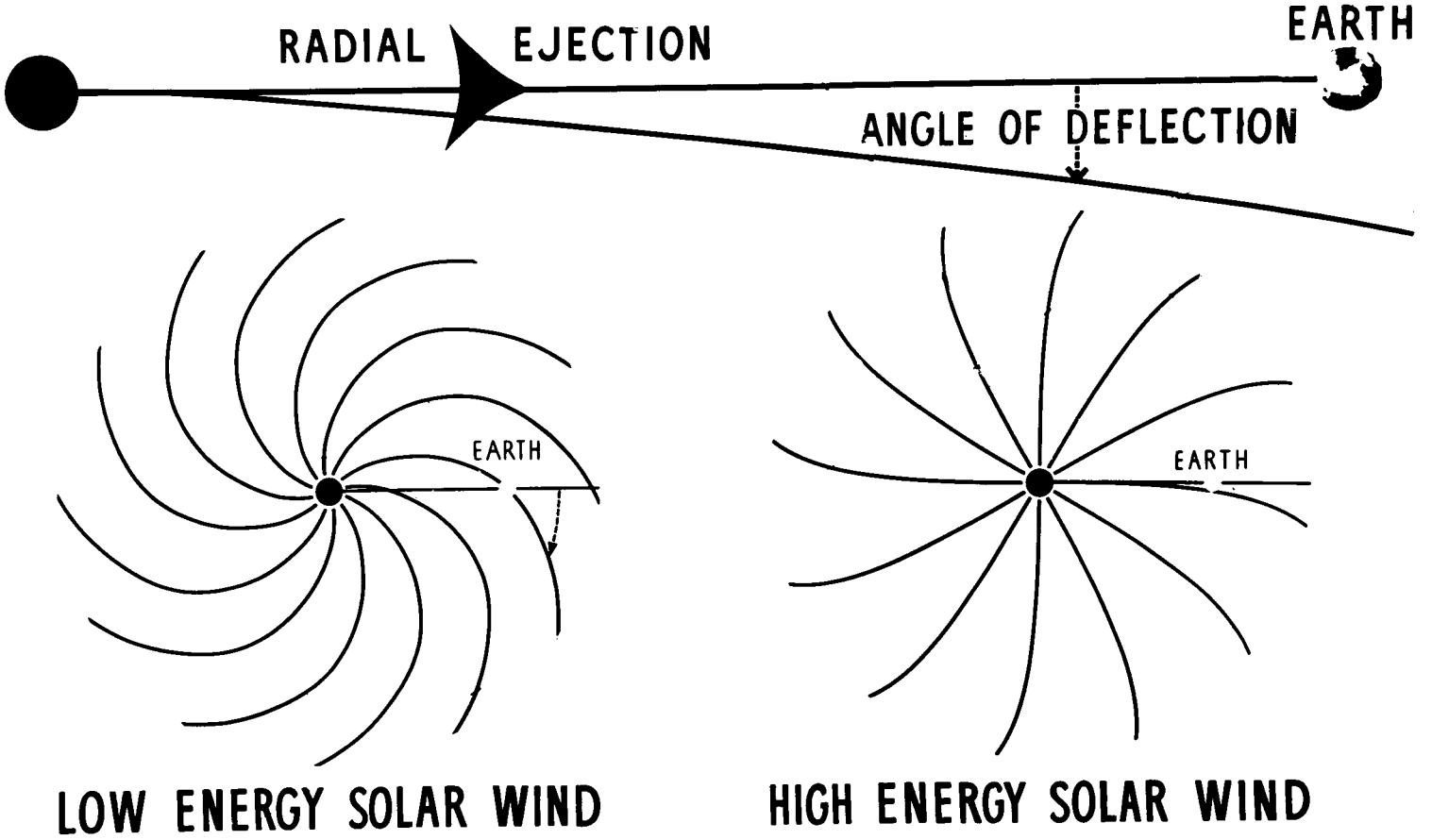

Figure 12

THEORETICAL INTERPLANETARY MAGNETIC FIELD STREAMING ANGLE

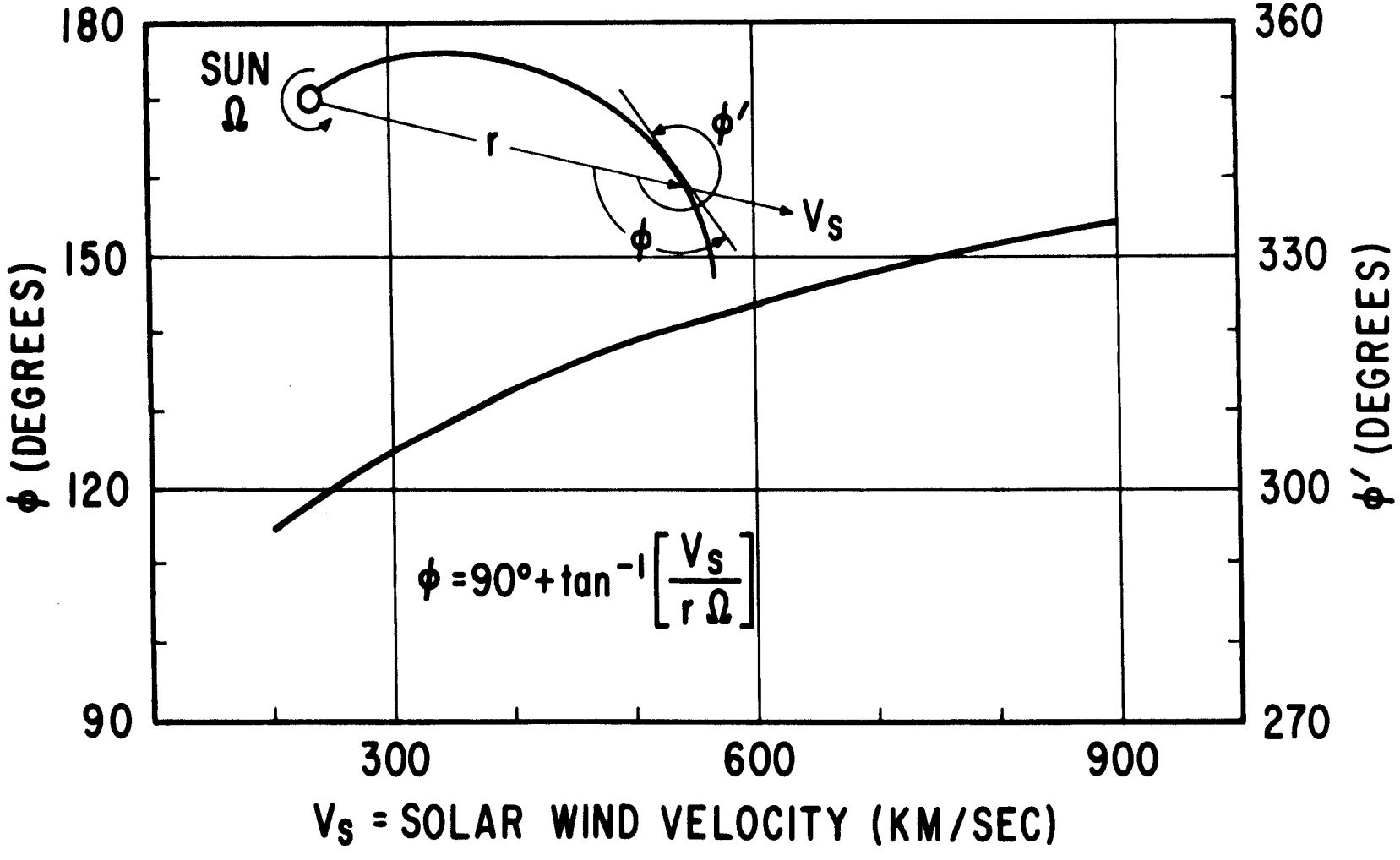

Figure 13

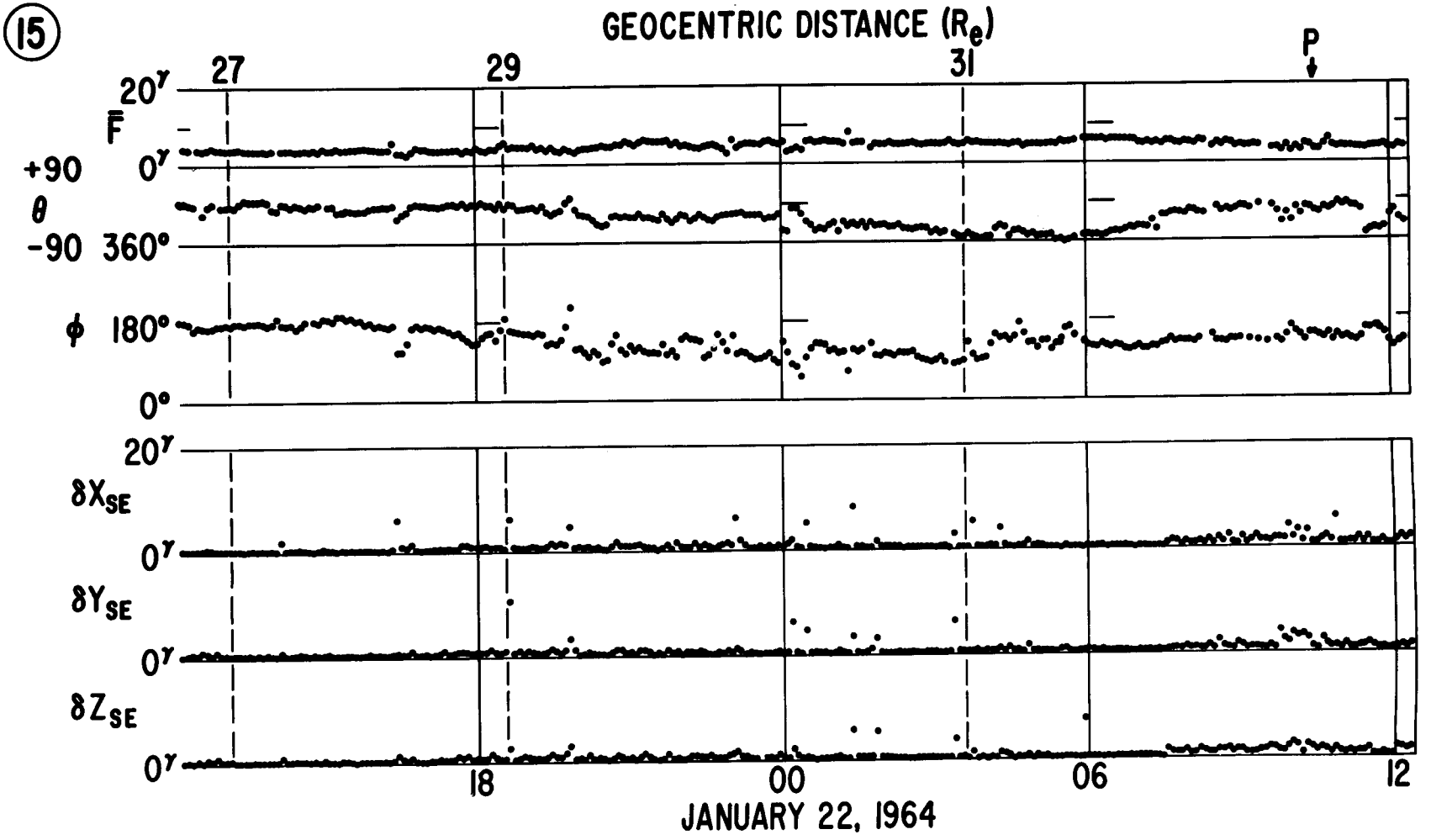
15
GEOCENTRIC DISTANCE (R_e)
27
29
31
P
20γ
F
0γ
+90
θ
-90
360°
φ
180°
0°
20γ
δX_SE
0γ
δY_SE
0γ
δZ_SE
0γ
18
00
06
12
JANUARY 22, 1964

Figure 14

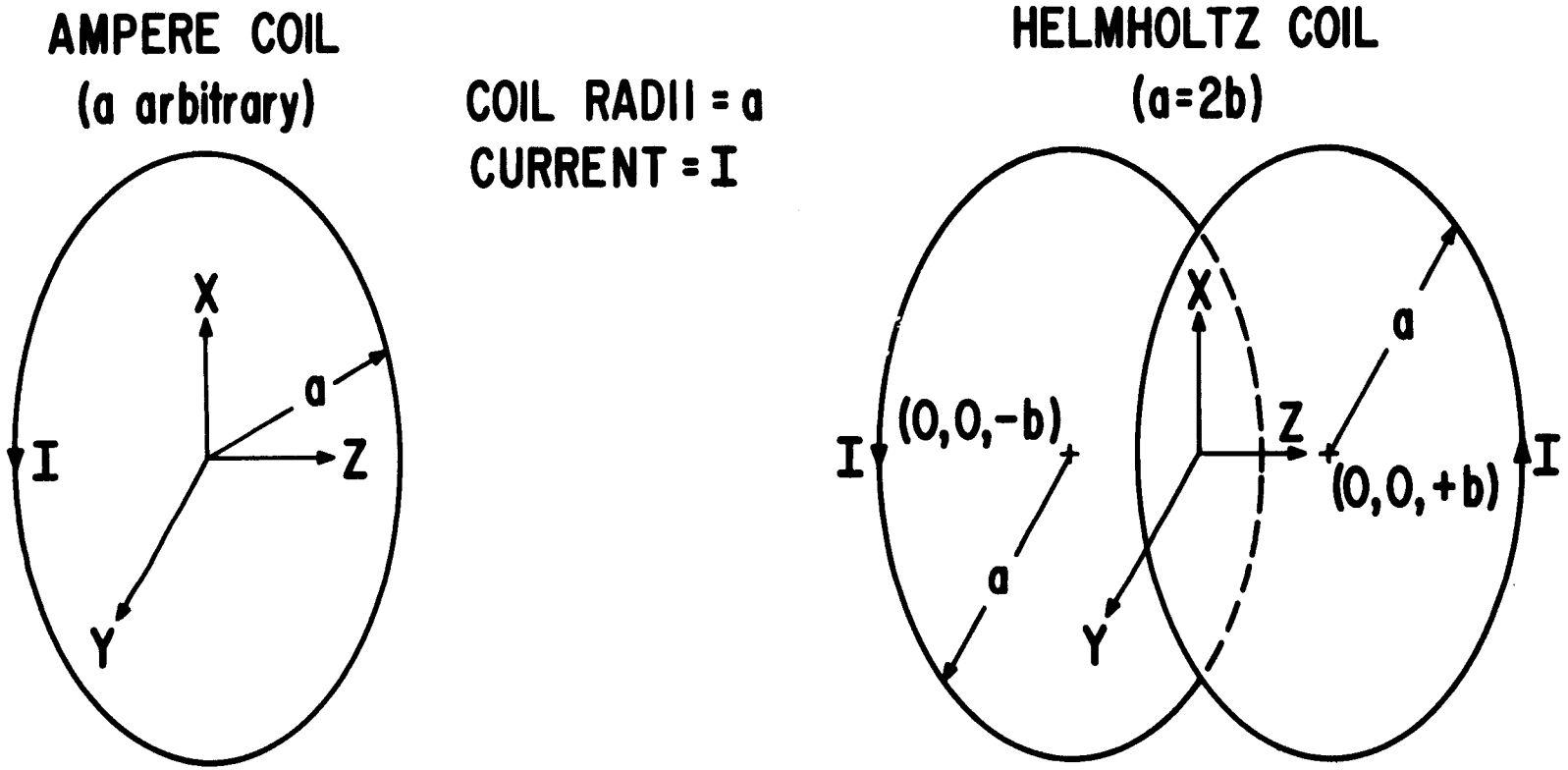

ELEMENTARY COIL SYSTEM GEOMETRIES

Figure 15

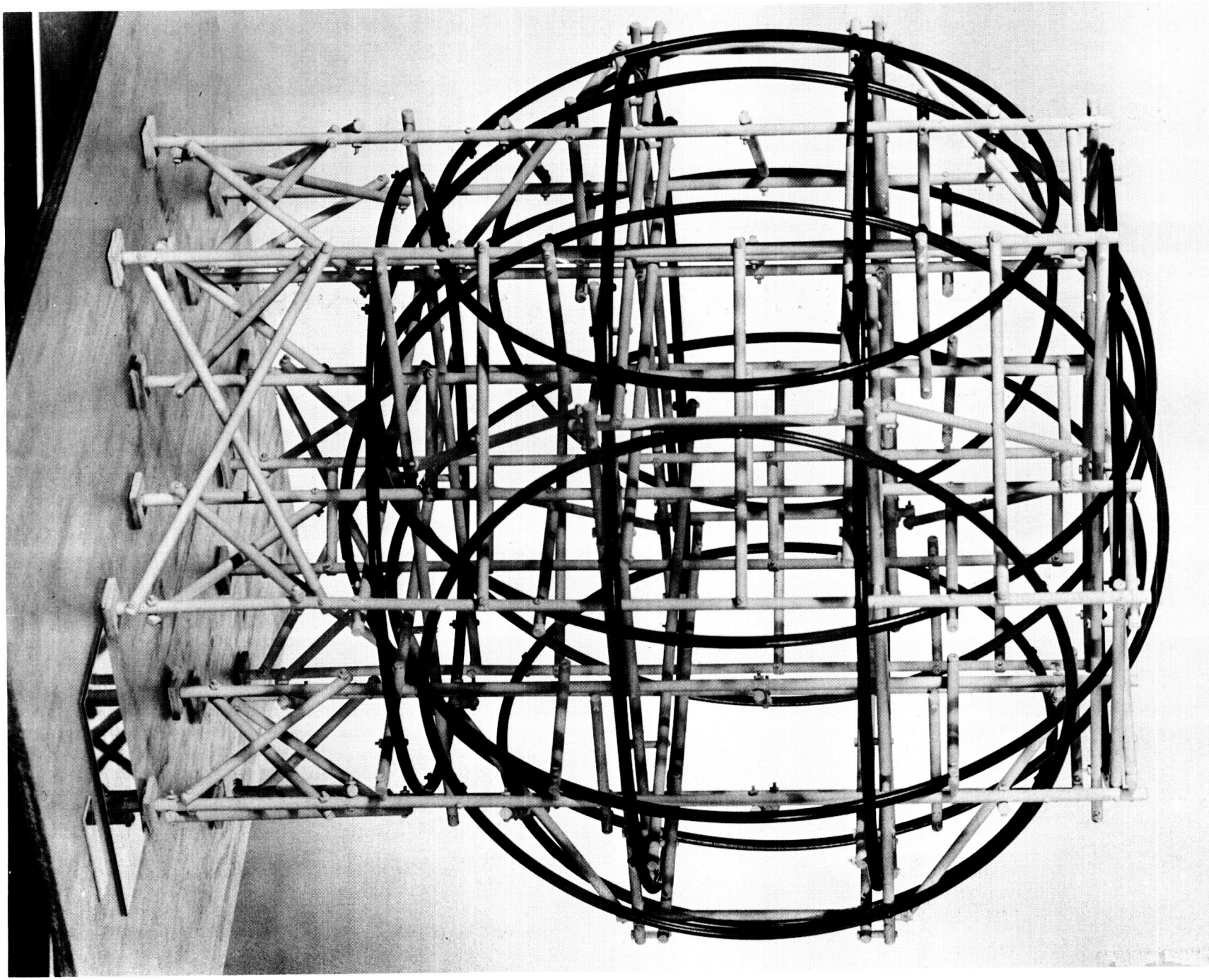

Figure 16

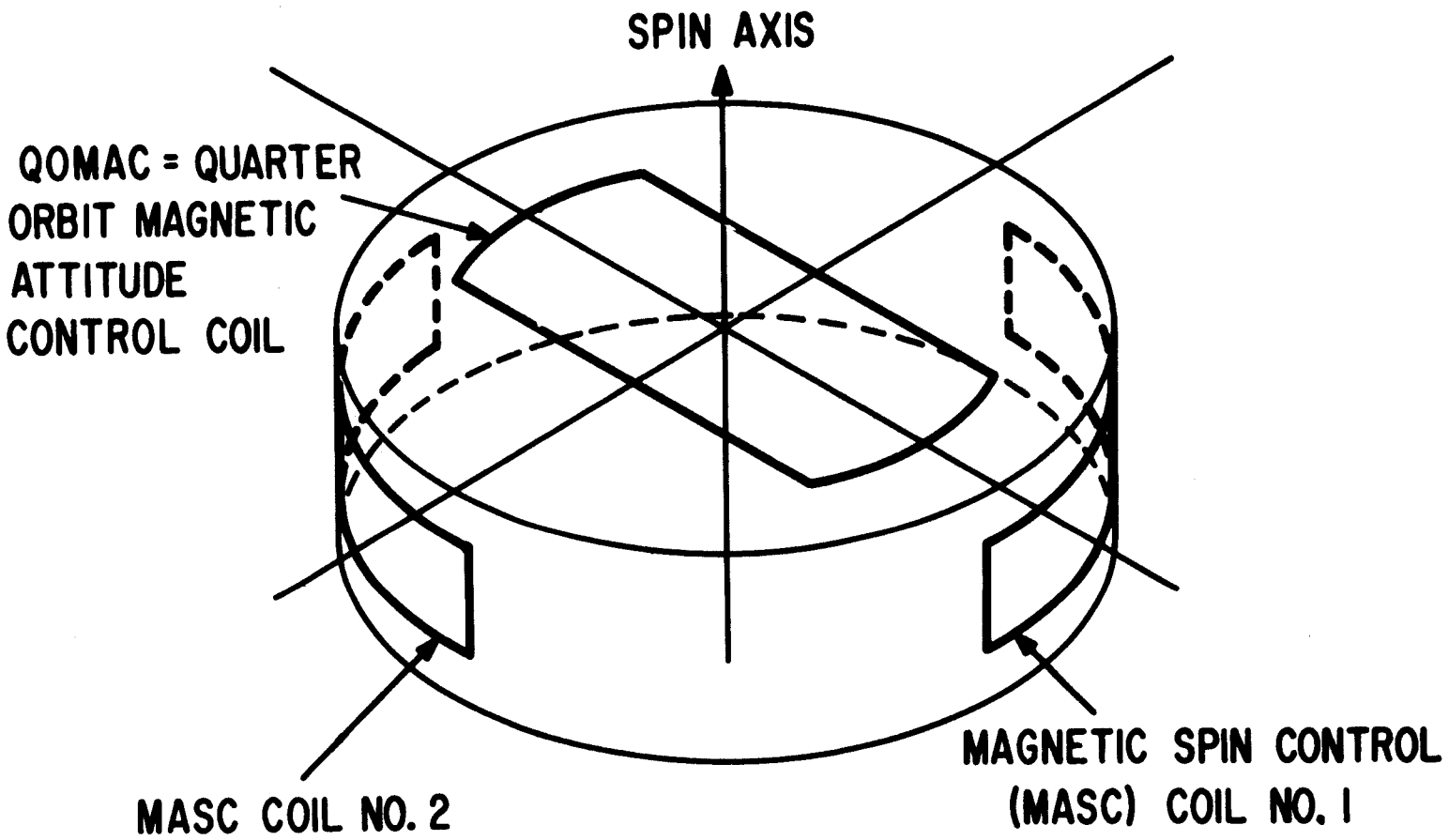

TIROS ACTIVE ATTITUDE CONTROL SYSTEM

Figure 17